Nanoscale

The Nanoscale Leidenfrost Effect

SCHOLARONE™
Manuscripts

The Nanoscale Leidenfrost Effect

Jhonatam Rodrigues[1] and Salil Desai[1,2,*]

Department of Industrial & Systems Engineering, North Carolina Agricultural & Technical State University, Greensboro, NC 27411, USA.

[2] Wake Forest Institute for Regenerative Medicine, Wake Forest School of Medicine, Winston–Salem, NC 27157, USA.

*Corresponding author: Salil Desai, sdesai@ncat.edu, +1-336-285-3725.

1

Abstract

Nanoscale evaporation of liquids plays a key role in several applications including cooling, drag reduction and liquid transport. This research investigates the Leidenfrost effect at the nanoscale as a function of substrate material, droplet size and temperature using molecular dynamics models. Water droplets ranging from 4 nm to 20 nm were simulated over gold and silicon substrates at 293 K, 373 K, 473 K, and 573 K. A significant increase in the kinetic energy (>5000kcal/mol) was observed for molecules in the vicinity of the substrates, indicating the presence of a vapor barrier layer between substrate and liquid. Higher droplet velocities were tracked for hydrophobic gold substrates as compared to hydrophilic silicon substrates indicating the influence of the surface wettability on the Leidenfrost effect. Droplets over silicon substrate had higher number of fluctuations (peaks and valleys) as compared to gold due to the cyclic behavior of vapor formation. An increase in the interfacial kinetic energies and translatory velocities (>10m/s) were observed as the droplet sizes reduced confirming the Leidenfrost effect at 373 K. This research provides understanding of the Leidenfrost effect at the nanoscale which can impact several applications in heat transfer and droplet propulsion.

1 Introduction

The Leidenfrost effect is characterized by a significant reduction in heat transfer from a heated body to liquids when the temperature of the body crosses a threshold [1] , known as the Leidenfrost Point (LFP) temperature. This phenomenon occurs when liquids are deposited on hot solid surfaces and a layer of vapor is formed in between the droplet and the substrate. This vapor layer provides a frictionless motion to the droplet isolating the substrate from the liquid and reducing the total heat transfer [2]. The Leidenfrost effect has been systematically explored for macro scale applications such as cooling [3], liquid transport [4] and drag reduction [5], however, needs further investigation at the nanoscale dimensions.

The use of nanoscale structures has been studied to increase the LFP temperature, given its criticality in cooling applications [6]. Sajadi S, et al. proposed a layered structure that would eliminate the Leidenfrost Point [7]. Hassebrook, A. et al. reported an increase in the Leidenfrost temperature by 200 °C [8] by growing nano/microstructures on a substrate. The Leidenfrost effect has been applied to minimize the drag on solid bodies moving within a liquid [6, 9]. Bain, R. et al. demonstrated that the Leidenfrost effect can be used to accelerate chemical reactions [10]. Shahriari, A. et al. applied an electric field to the interface of a substrate in order to promote wettability consequently increasing the Leidenfrost Point [11].

In spite of several investigations of the Leidenfrost effect at the macroscale, there is a limited body of knowledge that explains the phenomenon at the nanoscale regime. The experimental analysis of the Leidenfrost phenomenon at the nanoscale regime is non-trivial as the nanodroplets are below the optical resolution. Nanoscale droplets have extremely fast evaporation kinetics depending on the initial size of the droplet. In recent years, attempts are being made to study the interfacial fluid-structural behavior using environmental scanning

electron microscopy for stationary nanodroplets [12]. However, this approach is being attempted for nanodroplets above the size of 400 nm which are composed on non-volatile fluids such glycerin, oil etc. To the best of our knowledge, currently, there are no experimental tools that can image fast moving nanoscale droplets at the Leidenfrost temperatures. Thus, several research groups have used molecular models to investigate the interaction of nanofluids with different substrates [13-19].

The interaction of heated nanodroplets with substrates has an ever-increasing number of applications. Nanoscale fabrication processes such as chemical vapor deposition and physical vapor deposition utilize nanoscale species of materials that are deposited on heated substrates to form 2D and 3D nanoscale features [20, 21]. Researchers at the National University of Singapore have fabricated ultrathin ribbon-shaped molybdenum disulphide structures by the reaction of precursor materials at ~700°C on a clean crystal surface [22]. This reaction resulted in the formation of nanodroplets which travelled at high velocities forming ribbon-like structures, unlike the traditional cylindrical or spheroidal structures. Herein, the random motion of the deposited nanodroplets from the precursor source to the substrate is dictated by the underlying wettability and thermal gradients of the nanodroplets. Zagoranskiy et al. have guided self-organization of heated nanodroplets induced by nanosecond IR laser radiation on a sapphire substrate [23]. Our research will shed light on the spreading behavior of heated nanodroplets which have a significant impact on the deposition of thin-films and nanoscale structures for photonic, sensor, and biomedical devices. In addition, other droplet based processes involve the use of atomized jets of nanodroplets to form nanomaterials based on condensation, nucleation, and growth on heated substrates [24, 25]. Charged nanodroplets of aqueous media were deposited on Si wafer at 873K to generate nanoparticles for sterilization of yeast fungi [26]. A patented scalable nano/micro droplet deposition process has been developed wherein, microscale droplets are irradiated with lasers

to transform them into nanodroplets on-the-fly [27]. The nanodroplets are then deposited on heated substrates for the formation of nanoscale structures. The initial impact, spread dynamics and motion of the nanodroplet on the heated substrate represents the Leidenfrost phenomena at the nanoscale regime. Heated nanodroplets have also been used to encapsulate chemotherapy drugs and contrast agents that are further irradiated with lasers for treatment of tumors and targeted molecular imaging [28, 29].

As stated above, heated nanoscale droplets undergoing temperature gradients (Leidenfrost effect) have been implemented in multiple applications. Thus, a detailed atomistic investigation of these nanodroplets is necessary to reveal the complex transport phenomena, which can be further exploited for tuning properties of nanomaterials. In addition, we believe that the study of the nanoscale Leidenfrost effect will serve as a basis to design a family of applications for anti-dragging surfaces, self-propelling droplets, self-assembled nano structures, and cooling applications.

In this research, the Leidenfrost effect is characterized at the nanoscale with respect to the kinetic energy, droplet velocity, and temperature profile. Our results report higher kinetic energies and corresponding higher droplet velocities that are inversely proportional to the size of the nanodroplets. We confirm the presence of Leidenfrost point (LP) for nanoscale droplets at 373K which is lower than the recorded (LP) at the microscale [30]. Water nanodroplets ranging from 4 nm to 20 nm were simulated with respect to hydrophobic gold and hydrophilic silicon nitride substrates, respectively. This research lays the foundation for understanding the Leidenfrost effect at the nanoscale based on variations in substrate wetting, droplet size and temperature with a potential to impact several applications.

2 Materials and Methods

Nanoscale Molecular Dynamics (NAMD) source code was used to execute the simulations. NAMD is a high-performance code for parallel computing [31] and compatible

with most force fields for the commonly available CHARMM [32] package. Visual

Molecular Dynamics (VMD) was used to pre and post-process the molecular models. NAMD

and VMD were developed by the Theoretical and Computational Biophysics Group in

Beckman Institute for Advanced Science and Technology at the University of Illinois at

Urbana-Champaign [33]. The simulations were run on GPU [34] computing resources

provided by XSEDE (K80, with 4992 cores) [35].

Spherical water nanodroplets with diameters of 4 nm, 7 nm, 10 nm, 15 nm and 20 nm

were modeled using 1,108, 5,951, 17,267, 58,462 and 138,537 molecules, respectively. These

spherical droplets were placed tangent to the substrates while initializing the simulations. The

droplets were minimized for 20 ps and further attained their final equilibrium contact angles

with respective substrates. A TIP3P structure was used to represent the water molecules.

Gold and silicon substrates were used. The gold substrates had their molecules in a face-

centered cubic (FCC) structure following a [1 0 0] crystal orientation. Figure 1 shows the MD

model of a 10 nm droplet over (a) gold (131°) and (b) silicon (86.6°) substrate at their

equilibrium contact angles, respectively.
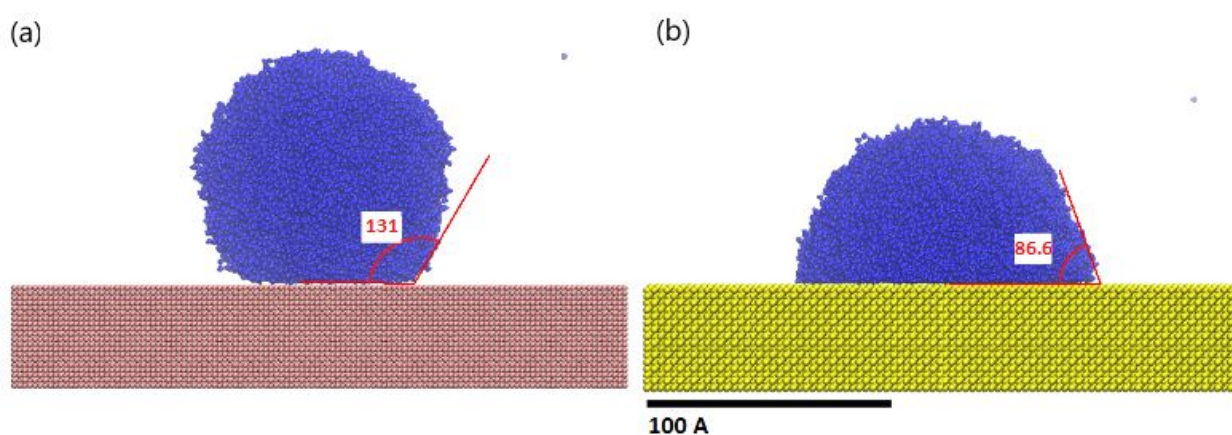
Figure 1. 10 nm water droplet over (a) gold and (b) silicon substrate in equilibrium

2.1 Force Fields

The direct-space interactions of temperature, pressure and electrostatic forces were

calculated using the Particle Mesh Ewald (PME). The electrostatic interaction was modeled

using Coulomb's law, while the Van der Waals (VdW) forces were modeled using Lennard-Jones 6-12 potential [36]. The potential energy from bending and stretching interactions were also included to represent water. All the interactions in the model were parameterized using a potential energy function compatible with CHARMM force fields. Equation (1) shows the functional form of the energy function.

$$U_{total} = U_{bond} + U_{angle} + U_{vdW} + U_{Coulomb} \qquad \text{Eq. (1)}$$

Where, U_{bond}, U_{angle} are the stretching and bending interactions, respectively.

$$U_{bond} = \sum_{\text{bonds } i} k_i^{bond}(r_i - r_{0i})^2 \qquad \text{Eq. (2)}$$

$$U_{angle} = \sum_{\text{bonds } i} k_i^{angle}(\theta_i - \theta_{0i})^2 \qquad \text{Eq. (3)}$$

The last two terms in the equation describe the Van der Waals and electrostatic potential.

$$U_{vdW} = \sum_i \sum_{j > i} 4\varepsilon_{ij}\left[\left(\frac{\sigma_{ij}}{r_{ij}}\right)^{12} - \left(\frac{\sigma_{ij}}{r_{ij}}\right)^6\right] \qquad \text{Eq. (4)}$$

$$U_{Coulomb} = \sum_i \sum_{j > i} \frac{q_i q_j}{4\pi\epsilon_0 r_{ij}} \qquad \text{Eq. (5)}$$

The parameters for equations 2-5 for water molecules (oxygen and hydrogen) were taken from the CHARMM force fields [37]. The parameters for gold and silicon substrates were adapted from Braun, R. et al. [38] and Mayo et al. [39], respectively. As the force of gravity does not influence interactions at the nanoscale [40], the interactions between the droplet and substrate are based on intermolecular interactions between pairs of molecules for the water droplet and the substrate atoms [41, 42]. These interactions are captured by two types of non-bonded potentials which include the Vander Waals and Coulomb potentials shown by equations 4 and 5. To explore the solid-liquid affinity the authors have run simulations with gold (hydrophobic) and silicon (hydrophilic) substrates with different sizes of droplets (4, 7, 10, 15 and 20 nm).

2.2 Simulation Parameters

A spherical volume of water was generated for nanodroplet from a pre-equilibrated water sphere using the solvate plugin in VMD. The solid substrates were generated using the inorganic builder in VMD. During the simulation, the substrate atoms had their coordinates fixed to their original position, while water molecules within the droplet were allowed to move freely. An integration time step of 2 fs was used to perform the simulations. The system position was recorded every 2000 steps. The VdW interactions were conducted with a cutoff of 12 Å and switching function starting at 10 Å. The long-range electrostatic interactions were calculated using the Particle Mesh Ewald (PME) method. The simulations were performed in an NVT ensemble, and a Langevin thermostat was used to control the temperature. All systems were minimized for 4000 steps of 2 fs and then equilibrated for 4 ns in an NVT ensemble. In the simulations of heated substrates, the system was thermalized to 293 K for 2500 steps, and the thermostat was set to a higher temperature acting only on the substrate for the remaining of the simulation.

2.3 Kinetic Energy

The Leidenfrost-effect occurs when a thin layer of vapor exists between a heated substrate and the liquid droplet. The thin vapor film significantly reduces the heat transfer between the substrate and droplet, retarding the boiling of the droplet. The droplet boiling is often accompanied by the random droplet motion. However, the motion itself might not indicate the presence of the Leidenfrost effect. In addition to the random motion, it is important to demonstrate that: (1) the droplet presents vapor and liquid phases and (2) the vapor phase lies trapped in between the substrate and the liquid phase.

The presence of these two conditions was verified by tracking the kinetic energy of the droplet molecules at the fluid-substrate interface. The simulation volume was divided into slices parallel to the substrate surface, and the average kinetic energy of the molecules in each

layer was calculated using the MD energy module in NAMD. Figure 2 illustrates the scheme used to compute the kinetic energy across different layers from the substrate. Each layer was set to a height of 0.5 Å.
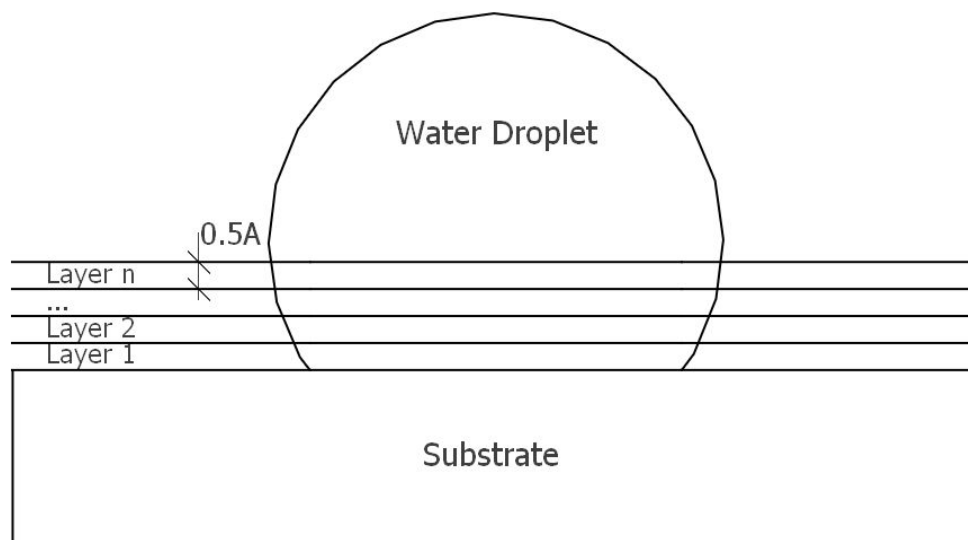
Figure 2. Schema of the division of layers used to compute the kinetic energy normal to the substrate. The average kinetic energy of molecules within the layer was calculated as a function of the distance away from the substrate.

In addition, the average kinetic energy of each layer was plotted against time. Thus, it was possible to track the progression of the kinetic energy of specific layers and to isolate the timeframes where vapor and liquid phases were present. One of the significant findings of this work is the observation of the Leidenfrost effect at 373 K, which is significantly lower than the one observed at the microscale [30]. To study this hypothesis, the gradients of kinetic energy at the droplet-substrate interface were studied for different droplet sizes, substrate types, and temperature as listed in Table 1.

Table 1. Evaluations of the kinetic energies for different droplet sizes, substrate types and temperatures

Index	Temperature (K)	Substrate	Droplet size (nm)
1	293	Au	4
2	293	Au	10
3	293	Si	4

4	293	Si	10
5	373	Au	4
6	373	Au	7
7	373	Au	10
8	373	Au	15
9	373	Au	20
10	373	Si	4
11	373	Si	7
12	373	Si	10
13	373	Si	15
14	373	Si	20

2.4 Density profile

The water density was sampled by dividing the simulation volume in a grid of 1 Å cubic bins. The atomic density was calculated at each grid point. To perform the calculations, each atom was replaced by a normalized Gaussian distribution with standard deviation equal to the atomic radius. The density map was created by summing the various Gaussians in the grid. The density maps were set up for every frame of the simulations using the *volmap* script from VMD. Liquid water has an atomic density of approximately 0.096 atoms/Å^3 between 293 K and 373 K [43]. The phase boundary between water and vapor occurs at 50% of the atomic density of liquid water, therefore if a simulation volume had less than 0.048 atoms/bin it was considered as vapor. The density profile was used to compute the percentage of the initial liquid water present in the droplet. This was tracked as the simulation progressed for each scenario presented in Table 1.

2.5 Droplet Displacement and Velocities

Droplets subjected to the Leidenfrost effect tended to move randomly over the substrate. To analyze the droplet movement, the center of mass of the water droplet was calculated for each frame of the simulation. The center of mass was computed as the weighted average position of the atoms in the droplet. The center of mass was tracked through all simulation frames creating a graphical representation of the trajectory of the droplet. The velocity of the droplet was calculated as the distance between of center of mass

for two consecutive frames divided by the interval of time between two frames (5ps = 2500 steps/frame x 2 fs/step). Velocities of droplets ranging from 4 nm to 20 nm over silicon and gold at 373 K, 473 K, and 573 K are presented in this work. A detailed trajectory analysis is presented for 4 nm droplet deposited over gold and silicon substrates at 473 K.

2.6 Temperature

The temperature of the droplet was measured for 4 nm and 10 nm droplets over gold and silicon substrates heated at 293 K, 373 K, 473 and 573 K. The Leidenfrost effect reduces the heat diffusion from the substrate to the droplet. This research intends to establish a relationship between droplet size and substrate material to determine optimal combinations that can initiate the Leidenfrost effect at nanoscale dimensions.

3 Results and Discussion

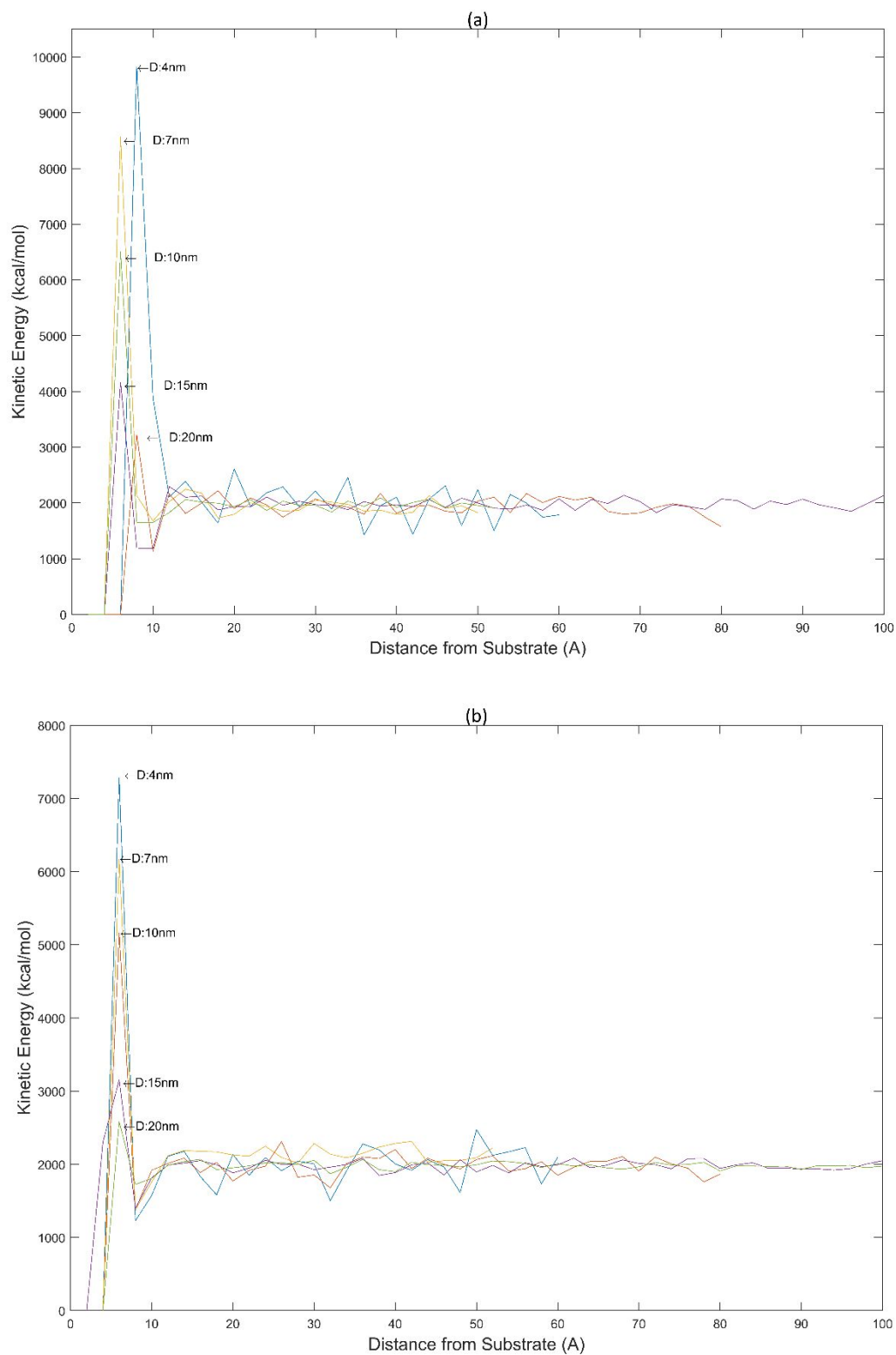## 3.1 Kinetic Energy

To investigate the location of vapor formation at the droplet and substrate interface, the kinetic energy of droplet molecules was tracked in close proximity of the substrate. Figure 3 shows the graph of the kinetic energy of water molecules (in vapor form) at layers closer to the substrate, for a 4 nm water droplet over a gold substrate at 373 K.
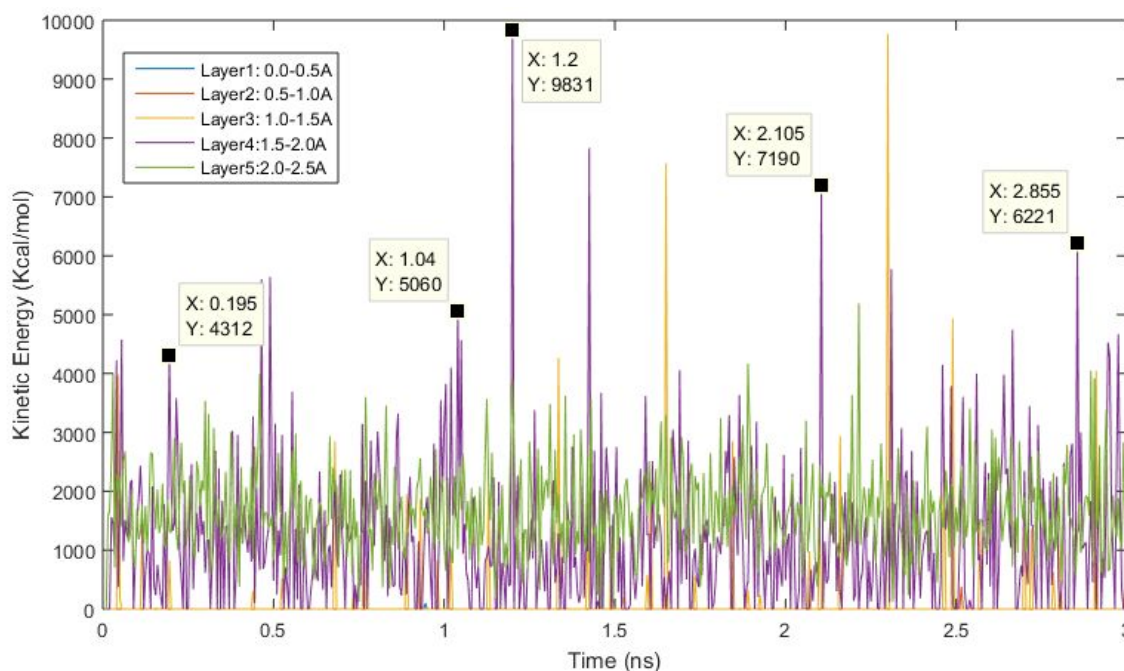
Figure 3. The average kinetic energy of water molecules in the first 5 layers of a 4 nm water droplet over a gold substrate at 373 K. Legends - X is the simulation time and Y is the kinetic energy in kcal/mol.

Layers 1 and 2 cannot be seen in Figure 3 as their kinetic energies are zero for most of the simulation time. Layer 3 presents sporadic peaks in the kinetic energy but the average energy is zero for a significant part of the simulation. This is due to the fact that for extended periods of the simulation these layers contain no vapor molecules. Thus, for layers 1 through 3, the van der Waal's interactions repel the water molecules from the substrate molecules at shorter distances. Layers 4 and 5 present a varying energy level throughout the simulation. Layer 4, represents atoms between 1.5 Å and 2.0 Å from the substrate and shows the highest peaks in energy. Figure 4 illustrates the kinetic energies of nanodroplets (ranging 4 nm to 20 nm) over gold and silicon substrates at 373 K. The kinetic energy was plotted as a function of the distance of the layers from the substrate.

Figure 4. Kinetic energy during vapor formation for 4 nm, 7 nm, 10 nm, 15 nm and 20 nm droplets on (a) gold and (b) silicon substrates at 373K.

As can be seen in the figures, the 4nm droplet has the highest kinetic energy peak (around 10000 kcal/mol) at 373 K followed by the larger sized droplets. This rapid rise in

13

kinetic energy is only seen at distances closer to the substrate (< 5 – 10 A) indicating the presence of vapor layer as explained in Figure 3. The rest of the layers of droplet away from the substrate have a much lower kinetic energy (around 2000 kcal/mol) which resemble the vibrational energy of the molecules in the droplets. It is important to note that as the droplet size increases there is a reduction in the kinetic energy peaks indicating that at substantially larger drop sizes the Leidenfrost effect would cease to exist at 373 K.

3.2 Volume Reduction

The density profile of the droplet was computed to identify the liquid core and vapor periphery. Figure 5 shows the proportion of water molecules in a liquid state for (a) a 4 nm droplet and (b) a 10 nm droplet over gold and silicon substrates at 293 K and 373 K, respectively.
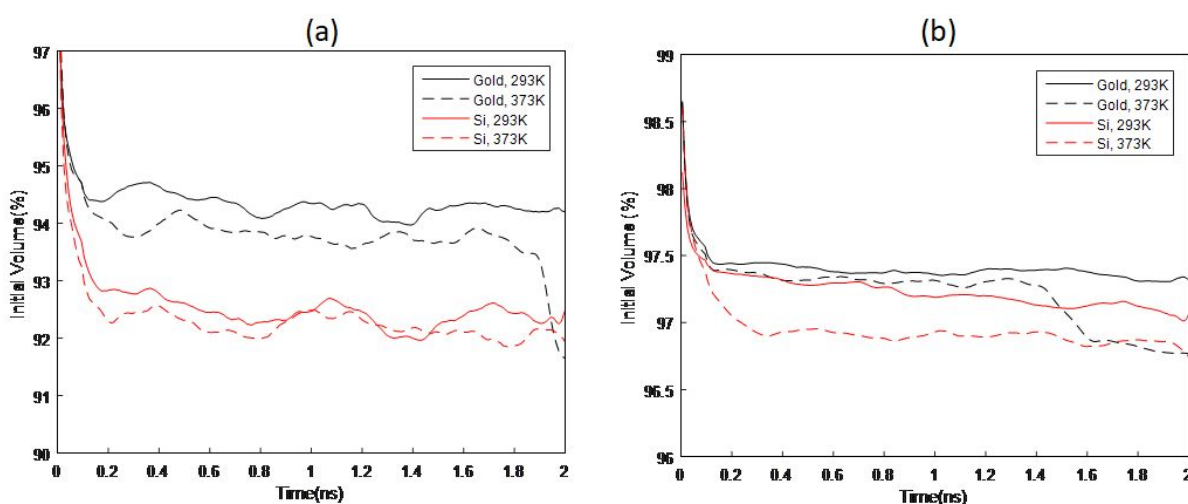
Figure 5. The proportion of water molecules at liquid state for (a) 4 nm and (b) 10 nm droplets over gold and silicon substrates.

At the beginning of the simulation, all droplets have 100% of water molecules in the liquid state. Shortly after the simulation starts, the proportion of water molecules starts to drop. At room temperature (293 K) and without heat transfer between the substrate and droplet, the droplet over silicon has a lower proportion of liquid water than the droplet over gold. Droplets over a flat silicon substrate have a lower contact angle (86.6°) than over gold substrate (131°). The hydrophilic surface of silicon induces higher substrate wettability

resulting in higher surface exposure of the droplet with the environment. Thus, higher surface exposure contributes to a higher rate of molecular diffusion from liquid to a vapor state because a greater proportion of the droplet is located at the surface of the droplet [44].

Analogously, droplets over the silicon substrate evaporate more rapidly than over gold substrate at an elevated temperature (373 K). However, the molecular count converges to a plateau over time with intermittent variations in the evaporation profile. This can be explained by the fact that after a vapor layer is formed at the fluid-substrate interface there is a drastic reduction in heat transfer between the droplet and substrates.

Similar to the 4 nm droplets, the 10 nm droplets show an initial reduction in liquid molecules on both substrates. Droplets on silicon substrate have a higher loss of vapor molecules as compared to gold. As compared to the 10 nm droplets, the 4 nm droplets have a higher reduction in liquid molecule count. This can be attributed to the higher surface to volume ratio for the 4 nm droplets as compared to 10 nm droplets. The water molecules on the surface are exposed to fewer hydrogen bonds and therefore require less energy to break free and diffuse away from the liquid droplet. Thus, smaller droplets evaporate proportionally faster as compared to larger droplets.

3.3 Droplet Propulsion Mechanism

A droplet undergoing the Leidenfrost effect over a flat substrate moves in random directions. This movement is induced by the formation of a vapor layer in between the droplet and substrate. The velocity at which the droplets moves over the substrate is dependent on different variables which include temperature of substrate, droplet size, and substrate material. Figure 6 shows the velocity of a 4 nm droplet over a gold substrate at 473 K, where, the label X is the time (ns) and Y is the velocity (m/s).

A specific pattern of droplet behavior was observed by correlating the peaks and valleys in the droplet velocity with the droplet position on the substrate as shown in figure 7.

The droplet is initially levitated by the vapor to propel it to a peak velocity. After attaining the highest velocity, the heat transfer between the substrate and droplet diminishes causing loss of vapor formation thereby, lowering its velocity until it slows down. After the droplet slows down (velocity valley), vapor builds between it and the substrate to cause the droplet to propel in a random direction. Thus, this cyclic behavior of the droplet is repeated causing the droplet to traverse in random directions as it moves across the substrate.

The velocity valley corresponds to the moment the droplet is in contact with the substrate, but then it is propelled by a vapor layer in another direction and levitated upwards, causing the sudden increase in velocity after the valley. The velocity peak seems to correspond to the moments the droplet is almost entirely suspended over a layer of vapor. Because the droplet is not in contact with the substrate, the heat transfer is diminished reducing the vapor formation. As a result, the droplet approaches to contact with the substrate, causing a sudden drop in velocity, corresponding to a velocity valley. Velocities valleys represent the rapid deceleration of the droplets wherein the droplet will be closest to the substrate. In the case of gold substrate, the fluid-substrate interaction is hydrophobic with lower surface exposure of the water molecules.
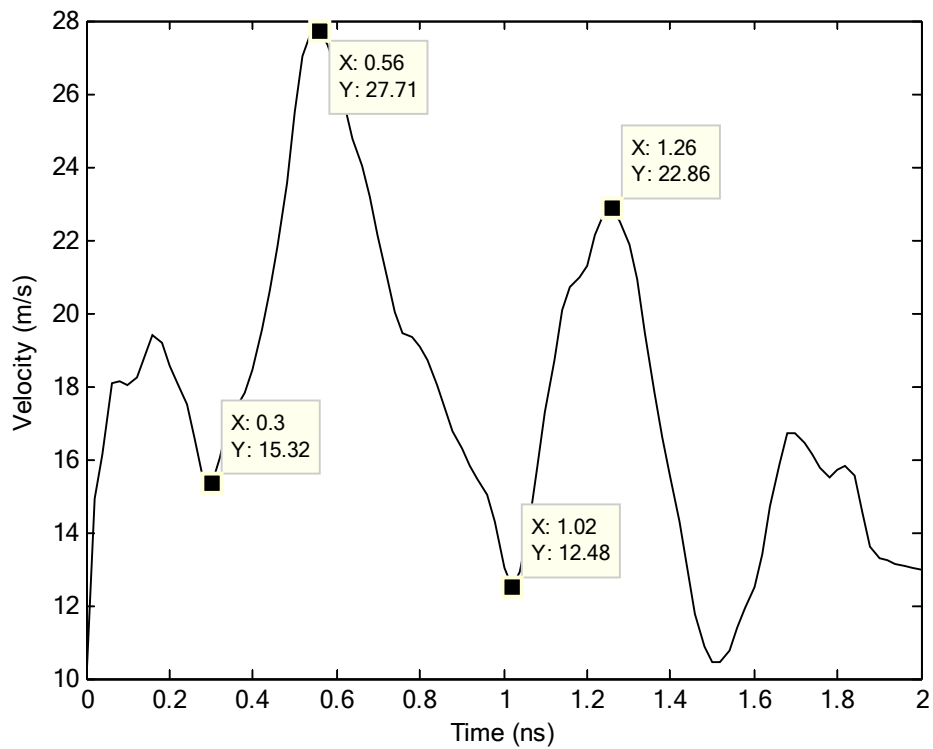
Figure 6. Droplet velocity profile (4 nm) over gold substrate at 473 K (X is time in ns and Y is velocity in m/s)
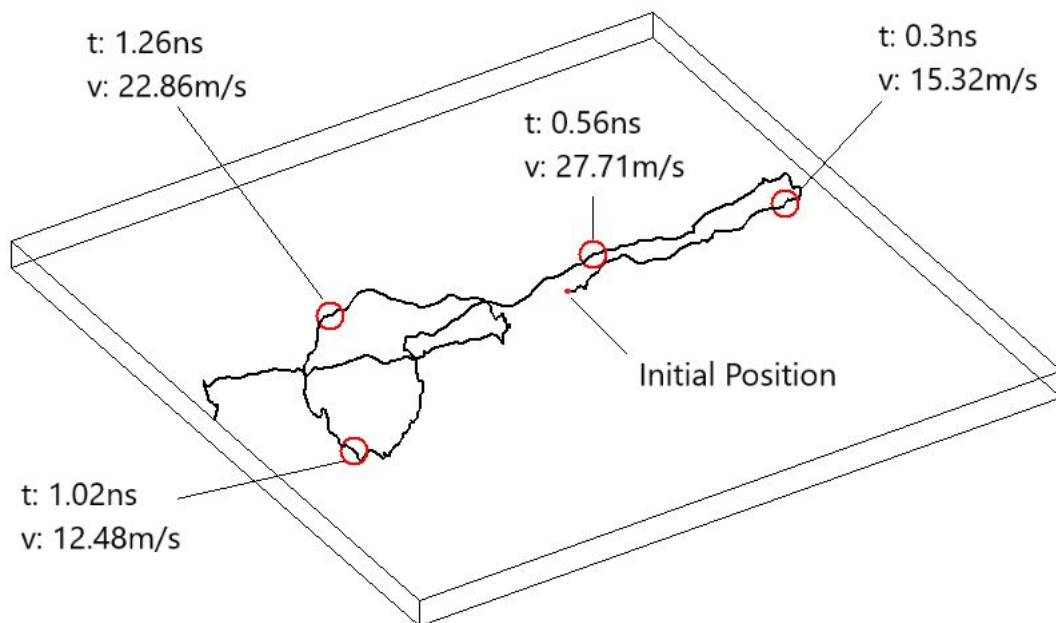
Figure 7. Trajectory path of 4 nm water droplet over a gold substrate at 473 K. The red circles indicate the position of the droplet at specific times with velocity valleys and peaks (figure 6).

17

For hydrophilic substrates such as silicon, the water-substrate interaction tends to decelerate the droplet motion. Figure 8 shows the front view of the trajectory path of a 4 nm droplet over silicon substrate at 473 K. The initial position of the droplet center is 20 Å from the substrate, but as the droplet spreads it rapidly reaches closer to the substrate.
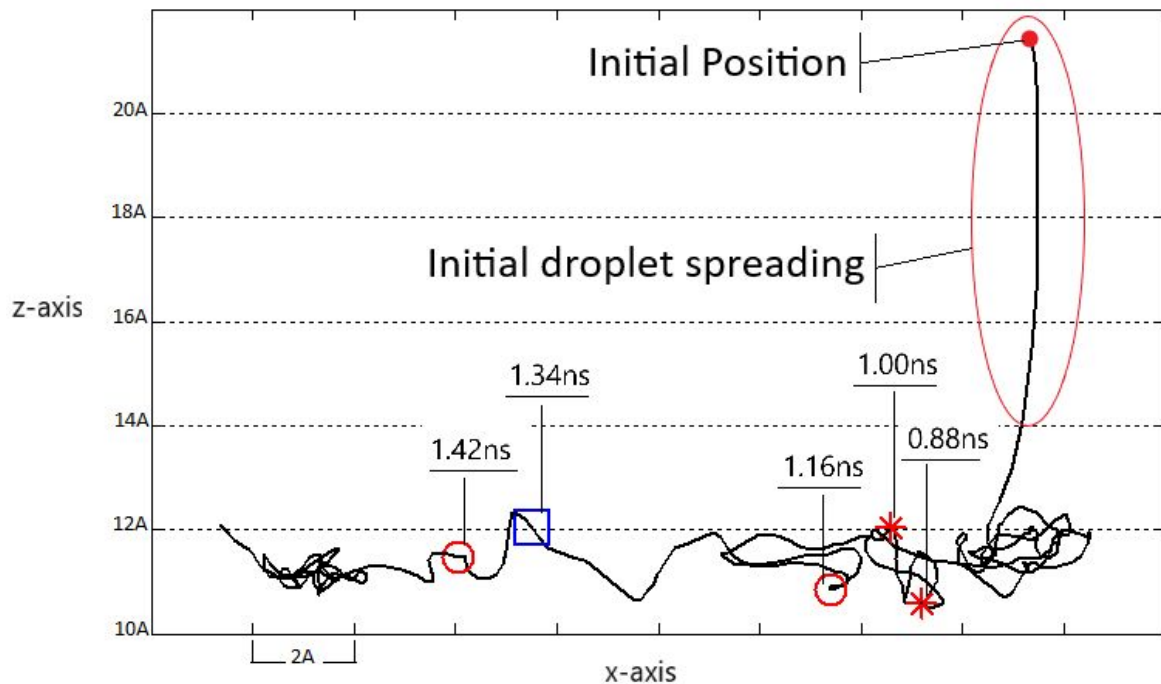

Figure 8. Front view of the trajectory path of a 4 nm droplet over silicon substrate at 473 K. The marks show the times when the droplet passed through that position. The '*' mark are points where the droplet velocity presented a valley; the 'o' are points where the droplet velocity reaches a peak, and the '□' mark illustrates a peak in the droplet distance from the substrate.

Figure 8 shows a velocity valley occurring at 0.88 ns where the droplet center of mass is closer to the substrate relative to other droplet positions. This velocity valley continues through 1.00 ns depicting a plateau profile (trough-like shape) after which the droplet starts to accelerate. In the case of silicon substrate, the droplet contact area is larger due to hydrophilic nature of the fluid-substrate interaction. The sustained contact results in higher vapor volume being generated that can transport the droplet for a longer period on the silicon substrate.

Thus, we observe prolonged regions of velocity valleys and peaks (plateau regions) for the silicon substrate that are not observed with the gold substrate.

Nanodroplets have a tendency for natural vibration about its mean position which is temperature dependent. In order to capture these harmonic oscillations, the droplet velocity at the center of mass were calculated at room temperature (293 K). Droplets at room temperature do not undergo the Leidenfrost effect and are stationary. It is important to note that these velocities do not represent droplet movement and are used as a base value to correct the actual velocities of droplets at higher temperatures undergoing the Leidenfrost effect. Figure 9 (a) and (b) show the velocities of 4 nm and 10 nm droplets over gold and silicon at different temperatures, respectively. The average velocity of the 4 nm droplets is consistently higher than the 10 nm droplet velocities due to inertial effects. The higher surface-to-volume ratio of smaller droplets also facilitates the breakage of hydrogen bonds in the droplet. This is evident as the slower moving 10 nm droplets present velocity peaks after 2 ns of simulation, whereas the 4 nm droplets present velocity peaks after a few picoseconds.

Figure 9 (c) and (d) show the correlation between higher interfacial kinetic energy with higher droplet velocities. Our results confirm findings in literature which indicate a substantial increase in droplet velocities with reduction in droplet sizes [45]. The higher droplet velocities occur due to the presence of higher kinetic energy of vapor molecules at the droplet-substrate interface which propel the droplets in random directions. In addition, larger sized nanodroplets would encounter relatively higher viscous effects slowing down their motion on the substrate [46, 47]. Thus, smaller drop sizes display higher tendency of Leidenfrost effect which diminishes as the droplet size increases.
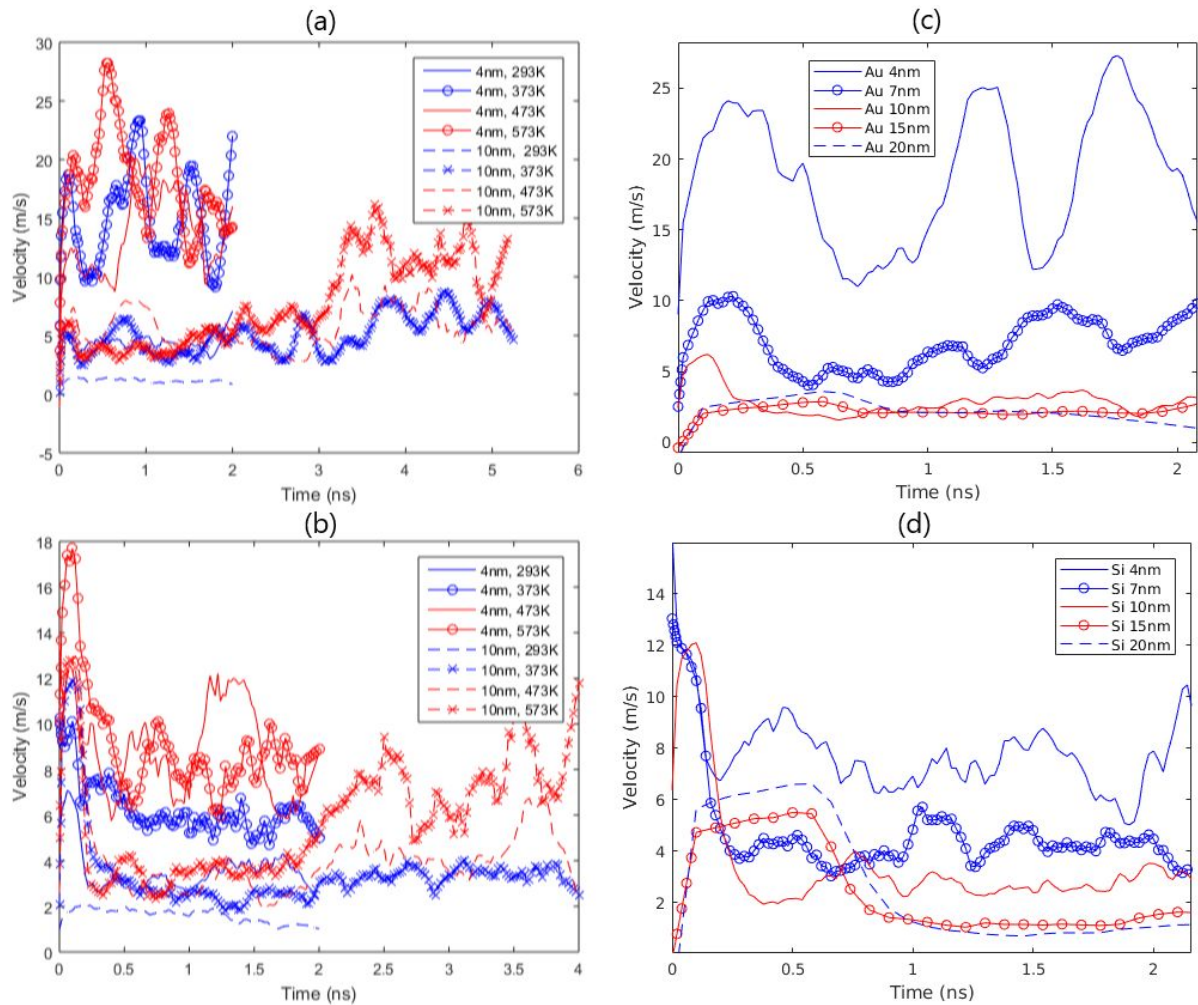
Figure 9. Velocities of 4 nm and 10 nm water droplets over (a) gold substrate and (b) silicon

substrate at 293 K, 373 K, 473 K, and 593 K. Velocities of 4, 7, 10, 15 and 20 nm over gold

(c) and silicon (d) at 373 K

The effect of substrate wettability is evident on the velocity of the droplets for all drop

sizes. Figure 9 (c) and (d) shows that hydrophobic (gold) substrate has consistently higher

velocities as compared to hydrophilic (silicon) substrate. The extended wetting behavior of

droplets on hydrophilic substrates provided higher interfacial resistance to motion [48].

Table 2 shows the influence of substrate type, droplet size and substrate temperature

on the velocities of droplets. The average velocities for 4 nm droplets are much higher as

compared to the 10 nm droplets for both the substrates as smaller droplets require less kinetic

energy to change its molecular arrangement [49]. Similarly, an increase in temperature of the substrate results in higher droplet velocities for both substrates and droplet sizes, respectively. Droplets over gold have a higher average velocity and standard deviation. This aligns with the fact that gold is a hydrophobic substrate which has fewer water molecules in contact thereby offering lower friction to the droplet movement. On the contrary, silicon is a hydrophilic substrate which offers higher friction and resistance to droplet movement. Thus, substrates with lower affinity with water molecules require lower propelling force and vapor formation to induce motion (Leidenfrost effect) in nanodroplets.

Table 2. Influence of substrate type, droplet size and substrate temperature on the velocities of nanodroplets

Temperature	Size	Gold (m/s)		Silicon (m/s)	
		Mean	Std. Dev.	Mean	Std. Dev.
293 K	4 nm	4.3	0.7	3.6	1.0
373 K	4 nm	14.7	3.9	6.3	1.2
473K	4 nm	13.3	3.8	8.9	2.1
573 K	4 nm	17.8	4.7	9.2	2.5
293 K	10 nm	1.1	0.1	1.5	0.3
373 K	10 nm	5.0	1.6	3.4	1.7
473 K	10 nm	5.6	1.8	4.2	1.9
573 K	10 nm	7.5	3.7	5.8	2.5

3.4 Temperature Profiles

Figure 10 (a) and (b) show the temperature variation of nanodroplets over gold and silicon substrates, respectively. This graph indicates that the droplet temperatures were always lower than the substrate temperature. This is because a significant portion of the water droplets were not in direct contact with the substrate and were in a liquid state (below 373 K).

The lower portion of the droplets that were in direct contact with the substrate resulted in vapor formation which further reduced the heat transfer between the substrate and the liquid water. The D^2 law describes the evaporation of droplets which are freely suspended in the ambient environment [50]. A reduction in the droplet size during droplet path-of-flight is dependent on several factors including droplet size, temperature, vapor pressure and ambient atmosphere [3]. However, in the case of droplets undergoing the Leidenfrost effect, the evaporation kinetics varies from the traditional D^2 law. The drop diameter change over-time can be approximated by a non-linear approximation in the form of the second degree polynomial [51]. However, the D^2 law modification is applicable to large sized droplets (centimeter sized droplets) and will need further modifications to track the evaporation kinetics for nanoscale droplets. To address this issue, the authors describe the temperature profiles of 4nm and 10nm droplets based on the balance of evaporation and heat accumulation within the nanodroplets.
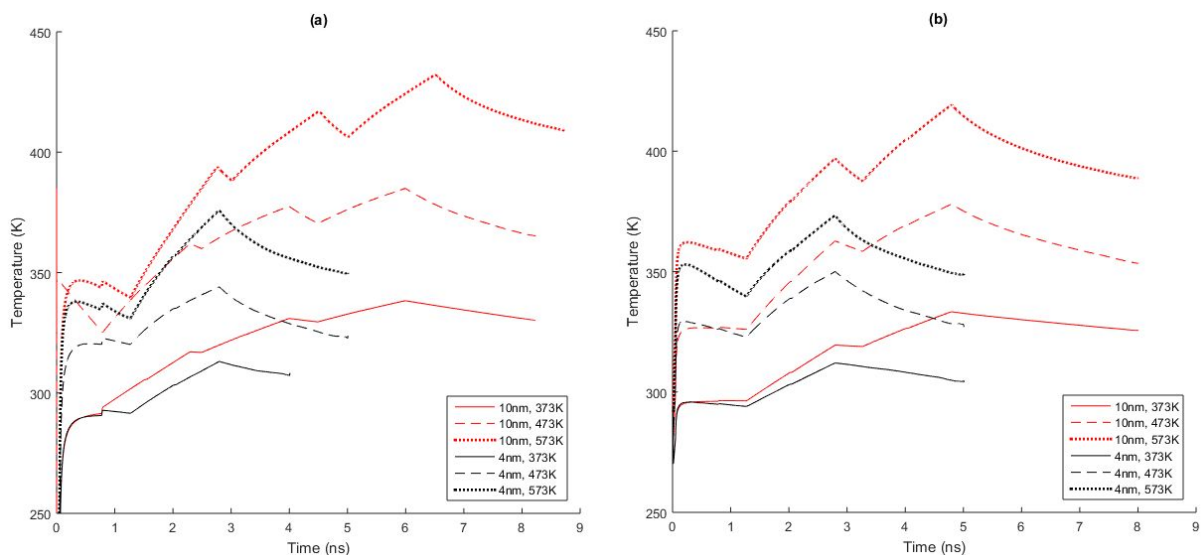
Figure 10. Temperature profiles of 4 nm and 10 nm water droplets over (a) gold substrate and (b) silicon substrate heated at 273 K, 373 K, 473 K, and 573 K.

The temperature of 10 nm water droplets was higher relative to the temperatures of 4 nm droplets for respective substrate temperatures. As previously discussed, the Leidenfrost

22

effect is more evident on smaller droplets, wherein the 4 nm droplets present rapid movements and peaks of velocities more frequently and at higher amplitudes as compared to 10 nm droplets. Moreover, the 10 nm droplets have prolonged contact with the heated substrate resulting in higher heat transfer from the substrate. This contributes to a higher percentage of the water molecules being heated resulting in elevated aggregate temperatures of the droplet. Also, the 4 nm droplets have a higher surface to volume ratio leading to rapid evaporation and thereby loss of kinetic energy as the vapor molecules separate from the droplet. Thus, the 4 nm droplet loses its latent heat of evaporation accounting for a lower temperature of the droplet.

The droplet temperature profiles also show a rise and fall pattern for the temperature of the droplet. This is because the droplet gains heat from the substrate before the formation of the vapor layer. Once the vapor layer is completely formed it levitates the drop and propels it in random direction. During this phase of droplet motion and levitation, the heat transfer from the substrate to the droplet is minimal. In addition, the droplet is losing vapor molecules due to evaporation from its surface which results in loss of kinetic energy and thereby temperature of the droplet. This is evident from all the saw-tooth pattern temperature profiles of droplets.

Similarly, droplets deposited over silicon substrates had a lower average temperature than droplets over gold as droplets deposited over silicon also evaporates faster. Droplets over silicon substrate have a higher spread due to hydrophilic substrate interaction. The higher surface area exposure allows for a higher heat transfer, which leads to higher evaporation rates for the silicon substrate.

4 Conclusions

This research investigates the Leidenfrost effect at the nanoscale with water droplets ranging from 4 nm to 20 nm deposited on heated gold and silicon substrates using molecular

dynamics simulations. The wettability of the substrates had an impact on the Leidenfrost effect at elevated temperatures (373 K, 473 K, 573 K). A significant finding of this research is the reporting of the Leidenfrost effect at 373 K. This temperature is much lower and in contrast with the Leidenfrost effect observed at 473 K for micro and macro scales. A rapid increase in the kinetic energy gradient normal to the surface of the substrate was observed for water molecules closer to the substrate. This phenomenon confirmed the presence of a vapor barrier layer retarding heat transfer from the substrate to the droplet. The droplet velocity was tracked wherein, the smaller droplets (4 nm) had higher velocities as compared to the larger droplets (20 nm) on both substrates. The droplet propulsion presented a profile of acceleration and deceleration with multiple velocity peaks and valleys. The velocity peaks corresponded to the droplet levitation by the vapor and attainment of higher velocities whereas, the valleys represented retardation and change in droplet direction. Droplets over silicon substrate had higher number of fluctuations (peaks and valleys) as compared to gold due to the cyclic behavior of vapor formation.

Smaller droplets (4 nm) had a faster evaporation rate as compared to the 10 nm droplet due to their higher surface to volume ratio. This resulted in higher frequency of velocity fluctuations in 4 nm droplets over the larger (10 nm) droplets. Droplets over silicon had a higher evaporation rate, than droplets over gold. This resulted in lower average temperatures for droplets on silicon versus gold substrate. A saw-tooth pattern of temperature rise and fall was observed for both substrates. These results reveal the interplay of different process parameters which include droplet size, substrate material and substrate temperature on the Leidenfrost effect at the nanoscale regime. This research lays the foundation to understand nanoscale fluid-structural interaction and heat transfer with applications in liquid transport, fluidic cooling, and nanoscale manufacturing processes.

Conflicts of interest

There are no conflicts to declare.

Acknowledgment

References

1. Eshuis P, van der Weele K, van der Meer D, Lohse D. Granular leidenfrost effect: Experiment and theory of floating particle clusters. Physical review letters. **95**(25), 258001 (2005).

2. Quéré D. Leidenfrost dynamics. Annual Review of Fluid Mechanics. **45**(197-215 (2013).

3. Kim H, Truong B, Buongiorno J, Hu L-W. On the effect of surface roughness height, wettability, and nanoporosity on leidenfrost phenomena. Applied Physics Letters. **98**(8), 083121 (2011).

4. Lagubeau G, Le Merrer M, Clanet C, Quéré D. Leidenfrost on a ratchet. Nature Physics. **7**(5), 395 (2011).

5. Vakarelski IU, Berry JD, Chan DYC, Thoroddsen ST. Leidenfrost vapor layers reduce drag without the crisis in high viscosity liquids. Physical Review Letters. **117**(11), 114503 (2016).

6. Buongiorno J, Ballinger R, Driscoll M, Forget B, Forsberg C, Golay M, Kazimi M, Todreas N, Yanch J. Technical lessons learned from the fukushima-daichii accident and

possible corrective actions for the nuclear industry: An initial evaluation. MIT Center for Advanced Nuclear Energy Systems, Cambridge, MA. (2011).

7. Sajadi SM, Irajizad P, Kashyap V, Farokhnia N, Ghasemi H. Surfaces for high heat dissipation with no leidenfrost limit. Applied Physics Letters. **111**(2), 021605 (2017).

8. Hassebrook A, Kruse C, Wilson C, Anderson T, Zuhlke C, Alexander D, Gogos G, Ndao S. Effects of droplet diameter and fluid properties on the leidenfrost temperature of polished and micro/nanostructured surfaces. J. of Heat Transfer. **138**(5), 051501-051507 (2016).

9. Saranadhi D, Chen D, Kleingartner JA, Srinivasan S, Cohen RE, McKinley GH. Sustained drag reduction in a turbulent flow using a low-temperature leidenfrost surface. Science Advances. **2**(10), (2016).

10. Bain RM, Pulliam CJ, Thery F, Cooks RG. Accelerated chemical reactions and organic synthesis in leidenfrost droplets. Angewandte Chemie. **128**(35), 10634-10638 (2016). doi:10.1002/ange.201605899

11. Shahriari A, Wurz J, Bahadur V. Heat transfer enhancement accompanying leidenfrost state suppression at ultrahigh temperatures. Langmuir. **30**(40), 12074-12081 (2014).

12. Méndez-Vilas A, Jódar-Reyes AB, González-Martín ML. Ultrasmall liquid droplets on solid surfaces: Production, imaging, and relevance for current wetting research. small. **5**(12), 1366-1390 (2009).

13. Hołyst R, Litniewski M. Heat transfer at the nanoscale: Evaporation of nanodroplets. Physical review letters. **100**(5), 055701 (2008).

14. Horne JE, Lavrik NV, Terrones H, Fuentes-Cabrera M. Extrapolating dynamic leidenfrost principles to metallic nanodroplets on asymmetrically textured surfaces. Scientific Reports. **5**(11769 (2015). doi:10.1038/srep11769

15. Cordeiro J, Desai S. The effect of water droplet size, temperature, and impingement velocity on gold wettability at the nanoscale. Journal of Micro and Nano-Manufacturing. **5**(3), 031008 (2017).

16. Marquetti I., Desai S., Orientation Effects on the Nanoscale Adsorption Behavior of Bone Morphogenetic Protein-2 on Hydrophilic Silicon Dioxide. RSC Advances, **9**, 906-916, (2019).

17. Marquetti, Izabele, and Salil Desai. "Molecular modeling the adsorption behavior of bone morphogenetic protein-2 on hydrophobic and hydrophilic substrates." Chemical Physics Letters **706**, 285-294, (2018).

18. Cordeiro, J., Desai S. The leidenfrost effect at the nanoscale. Journal of Micro and Nano-Manufacturing **4**(4), 041001, (2016).

19. Achhal EM, Jabraoui H, Zeroual S, Loulijat H, Hasnaoui A, Ouaskit S. Modeling and simulations of nanofluids using classical molecular dynamics: Particle size and temperature effects on thermal conductivity. Advanced Powder Technology. (2018).

20. Stelzner, Th, G. Andrä, E. Wendler, W. Wesch, R. Scholz, U. Gösele, and S. Christiansen. "Growth of silicon nanowires by chemical vapour deposition on gold implanted silicon substrates." Nanotechnology **17**(12), 2895, (2006).

21. Costa, José CS, Adélio Mendes, and Luís MNBF Santos. "Morphology of Imidazolium-Based Ionic Liquids as Deposited by Vapor Deposition: Micro-/Nanodroplets and Thin Films." ChemPhysChem **17**(14), 2123-2127, (2016).

22. Li, S., Lin, Y. C., Zhao, W., Wu, J., Wang, Z., Hu, Z., ... & Zhu, H. Vapour–liquid–solid growth of monolayer MoS2 nanoribbons. Nature materials, **17**(6), 535, (2018).

23. Zagoranskiy, Igor, Pierre Lorenz, Martin Ehrhardt, and Klaus Zimmer. "Guided self-organization of nanodroplets induced by nanosecond IR laser radiation of molybdenum films on sapphire." Optics and Lasers in Engineering **113,** 55-61, (2019).

24. Bortolani, F., and R. A. Dorey. "Synthesis of spherical lead zirconate titanate (PZT) nanoparticles by electrohydrodynamic atomization." Advances in Applied Ceramics, **108**(6), 332-337, (2009).

25. Brinley, E., K. S. Babu, and S. Seal. "The solution precursor plasma spray processing of nanomaterials." Jom 59, no. 7 (2007): 54-59.

26. Adachi, Motoaki, Masataka Kusumi, Masakazu Furuta, and Shigeki Tsukui. "Generation of nanodroplets and nanoparticles by ion-induced nucleation." Advanced Powder Technology 16, no. 5 (2005): 549-559.

27. Desai, Salil. "Methods and apparatus of manufacturing micro and nano-scale features." U.S. Patent 8,573,757, issued November 5, 2013.

28. Liu, Wei-Wen, Shu-Wei Liu, Yu-Ren Liou, Yu-Hsun Wu, Ya-Chuen Yang, Churng-Ren Chris Wang, and Pai-Chi Li. "Nanodroplet-vaporization-assisted sonoporation for highly effective delivery of photothermal treatment." Scientific reports **6,** 24753, (2016).

29. Kee, Allison Loo Yong, and Boon Mian Teo. "Biomedical applications of acoustically responsive phase shift nanodroplets: current status and future directions." Ultrasonics sonochemistry (2019).

30. Bernardin J, Mudawar I. The leidenfrost point: Experimental study and assessment of existing models. Journal of Heat Transfer. **121**(4), 894-903 (1999).

31. Phillips JC, Braun R, Wang W, Gumbart J, Tajkhorshid E, Villa E, Chipot C, Skeel RD, Kale L, Schulten K. Scalable molecular dynamics with namd. Journal of computational chemistry. **26**(16), 1781-1802 (2005).

32. Brooks BR, Bruccoleri RE, Olafson BD, States DJ, Swaminathan S, Karplus M. Charmm: A program for macromolecular energy, minimization, and dynamics calculations. Journal of computational chemistry. **4**(2), 187-217 (1983).

33. Humphrey W, Dalke A, Schulten K. Vmd: Visual molecular dynamics. Journal of molecular graphics. **14**(1), 33-38 (1996).

34. Marquetti, I., Rodrigues, J., & Desai, S. S. Ecological Impact of Green Computing Using Graphical Processing Units in Molecular Dynamics Simulations. International Journal of Green Computing (IJGC), **9**(1), 35-48, (2018).

35. J. Towns, T. Cockerill, M. Dahan, I. Foster, K. Gaither, A. Grimshaw, V. Hazlewood, S. Lathrop, D. Lifka and G. D. Peterson, Computing in Science & Engg., **16**(5), 62–74 (2014).

36. Grzybowski A, Koperwas K, Paluch M. Scaling of volumetric data in model systems based on the lennard-jones potential. Physical Review E. **86**(3), 031501 (2012).

37. MacKerell AD, Bashford D, Bellott M, Dunbrack R, Evanseck J, Field MJ, Fischer S, Gao J, Guo H, Ha Sa. All-atom empirical potential for molecular modeling and dynamics studies of proteins. The journal of physical chemistry B. **102**(18), 3586-3616 (1998).

38. Braun R, Sarikaya M, Schulten K. Genetically engineered gold-binding polypeptides: Structure prediction and molecular dynamics. Journal of Biomaterials Science, Polymer Edition. **13**(7), 747-757 (2002).

39. Mayo SL, Olafson BD, Goddard WA. Dreiding: A generic force field for molecular simulations. Journal of Physical chemistry. **94**(26), 8897-8909 (1990).

40. Sommer AP. Limits of the impact of gravity on self-organizing nanospheres. The Journal of Physical Chemistry B. **108**(24), 8096-8098 (2004).

41. Zhang J, Borg MK, Sefiane K, Reese JM. Wetting and evaporation of salt-water nanodroplets: A molecular dynamics investigation. Physical Review E. **92**(5), 052403 (2015).

42. Milchev A. in *Simulation of nanodroplets on solid surfaces: Wetting, spreading and bridging.* ed.by (Springer; 2006), 105-126, 2006.

43. VandeVondele J, Mohamed F, Krack M, Hutter J, Sprik M, Parrinello M. The influence of temperature and density functional models in ab initio molecular dynamics simulation of liquid water. The Journal of chemical physics. **122**(1), 014515 (2005).

44. Sharma P, Ganti S, Bhate N. Effect of surfaces on the size-dependent elastic state of nano-inhomogeneities. Applied Physics Letters. **82**(4), 535-537 (2003).

45. Li Q, Kang QJ, Francois MM, Hu A. Lattice boltzmann modeling of self-propelled leidenfrost droplets on ratchet surfaces. Soft Matter. **12**(1), 302-312 (2016).

46. Dupeux G, Le Merrer M, Lagubeau G, Clanet C, Hardt S, Quéré D. Viscous mechanism for leidenfrost propulsion on a ratchet. EPL (Europhysics Letters). **96**(5), 58001 (2011).

47. Dupeux G, Le Merrer M, Clanet C, Quéré D. Trapping leidenfrost drops with crenelations. Physical review letters. **107**(11), 114503 (2011).

48. Halverson JD, Maldarelli C, Couzis A, Koplik J. A molecular dynamics study of the motion of a nanodroplet of pure liquid on a wetting gradient. The Journal of chemical physics. **129**(16), 164708 (2008).

49. Wu C-D, Kuo L-M, Lin S-J, Fang T-H, Hsieh S-F. Effects of temperature, size of water droplets, and surface roughness on nanowetting properties investigated using molecular dynamics simulation. Computational Materials Science. **53**(1), 25-30 (2012).

50. Law C, Law H. A d2-law for multicomponent droplet vaporization and combustion. AIAA journal. **20**(4), 522-527 (1982).

51. Orzechowski T, Wciślik S. Analysis of d2-law in case of leidenfrost drop evaporation. Experimental Thermal and Fluid Science. **59**(230-237 (2014).
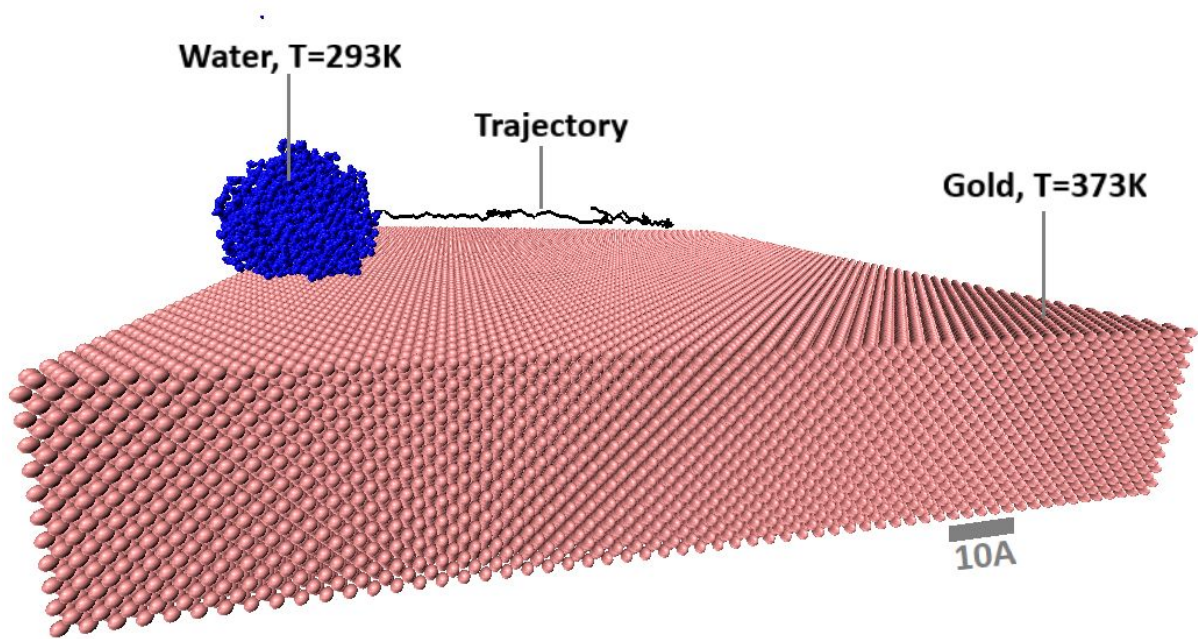
Droplet propulsion on gold substrate demonstrating the Leidenfrost effect at 373K